This is an open access article published under a Creative Commons Attribution (CC-BY) License, which permits unrestricted use, distribution and reproduction in any medium, provided the author and source are cited.

ACS APPLIED MATERIALS & INTERFACES

Research Article

www.acsami.org

# Mesoporous Vertical $Co_3O_4$ Nanosheet Arrays on Nitrogen-Doped Graphene Foam with Enhanced Charge-Storage Performance

Yuqin Zou,[†] Ian A. Kinloch,[‡] and Robert A. W. Dryfe*[,†]

[†]School of Chemistry and [‡]School of Materials, University of Manchester, Manchester M13 9PL, United Kingdom

Supporting Information

**ABSTRACT:** A hierarchical electrode structure, consisting of cobalt oxide and nitrogen-doped graphene foam (NGF), has been fabricated with the aim of achieving enhanced charge-storage performance. Characterization of the material via electron microscopy and Raman spectroscopy demonstrates that the $Co_3O_4$ nanosheets grow vertically on NGF and the nanosheets are mesoporous with pore diameters between 3 and 8 nm. The $Co_3O_4$/NGF electrode shows an enhanced charge-storage performance, attributed to the 3D hierarchical structure and the synergistic effect of $Co_3O_4$ and NGF. The present study shows that specific capacitances as high as 451 F $g^{-1}$ can be obtained, indicating that high-performance electrochemical capacitors can be made using electrode materials with advanced structures. The present electrode design can be readily extended to other electroactive materials and their composites.

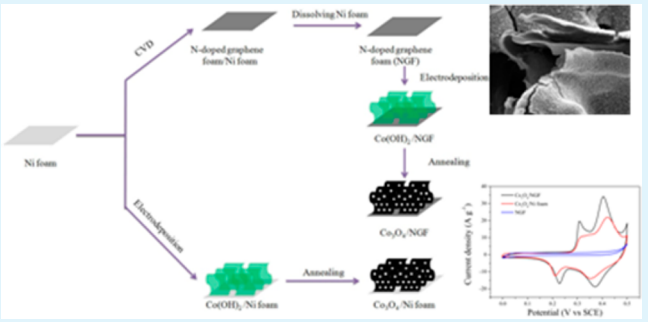


**KEYWORDS:** *cobalt oxide, hollow 3D structure, nitrogen-doped graphene foam, enhanced capacitive performance, charge storage*

## INTRODUCTION

Supercapacitors (SCs, also called electrochemical capacitors or ultracapacitors), represent a unique class of electrical energy storage devices, which have been extensively studied in recent years because of their high power density, fast charge–discharge rate, and long cycle life.[1] Several types of SCs can be catalogued depending on the charge storage mechanism as well as the active materials used.[1] Electrochemical double-layer capacitors (EDLCs) use high-surface-area carbon-based materials to achieve non-Faradaic storage of charge.[1] Other groups of SCs, known as pseudocapacitors (PCs) or redox supercapacitors, use fast and reversible surface, or near-surface, reactions for charge storage.[2] The charging and discharging behavior of pseudocapacitive materials (such as certain transition metal oxides[3] and electrically conducting polymers[4]) ) occurs on the order of seconds and minutes, which enhances the energy density without sacrificing too much of the power density.

$Co_3O_4$ has been widely investigated as a pseudocapacitive material with anticipation that it could be a replacement for $RuO_2$, because of its low cost, low environmental footprint, existence of a number of stable oxidation states and consequent high theoretical specific capacitance.[5] The significant capacitance is due to the formation of transition metal hydroxides during the charging process in alkaline electrolyte.[5] However, since metal oxide can also been used as the active materials for batteries, two underlying mechanism should be carefully distinguished. True SCs, compared to batteries, rely on distinct electrochemical processes. In the active oxide materials of lithium ion batteries, the insertion of $Li^+$ enables redox reactions in bulk electrode materials that are diffusion-controlled and can be slow. By contrast, supercapacitors store charge by adsorption of electrolyte ions onto the surface of electrode materials.[6] In the 1970s, Conway and others recognized that reversible redox reactions occurring at or near the surface of an appropriate electrode material lead to EDLC-like electrochemical features but the redox processes lead to much greater charge storage.[1] According to a recent report,[6] a pronounced redox peak in the voltammetry, can be an indication of pseudocapacitance, provided the peak voltage differences are small and remain so with increasing sweep rate. An alternative definition rests on the independence of the capacitance with voltage, i.e. the existence of a near-continuum of states associated with the intercalation and/or adsorption of ions to a structure. However, the above small separation of redox peaks is not strictly defined, and in fact many literature reports consider the active electrode materials as supercapacitor, even though the separation of peaks is on the order of 0.1 V.[7−11] The performance of PCs is mainly determined by the conductivity and surface area of the electrodes. Therefore, it is critical to enhance the conductivities of the active materials and increase the effective surface area of the electrode. Unfortunately, the traditional electrode preparation technique involves making a slurry of active material, polymer binder and solvent so that a large portion of the electroactive surface is blocked from contacting the electrolyte.

**Received:** June 9, 2015
**Accepted:** September 25, 2015
**Published:** September 25, 2015

 © 2015 American Chemical Society 

DOI: 10.1021/acsami.5b05095
*ACS Appl. Mater. Interfaces* 2015, 7, 22831−22838

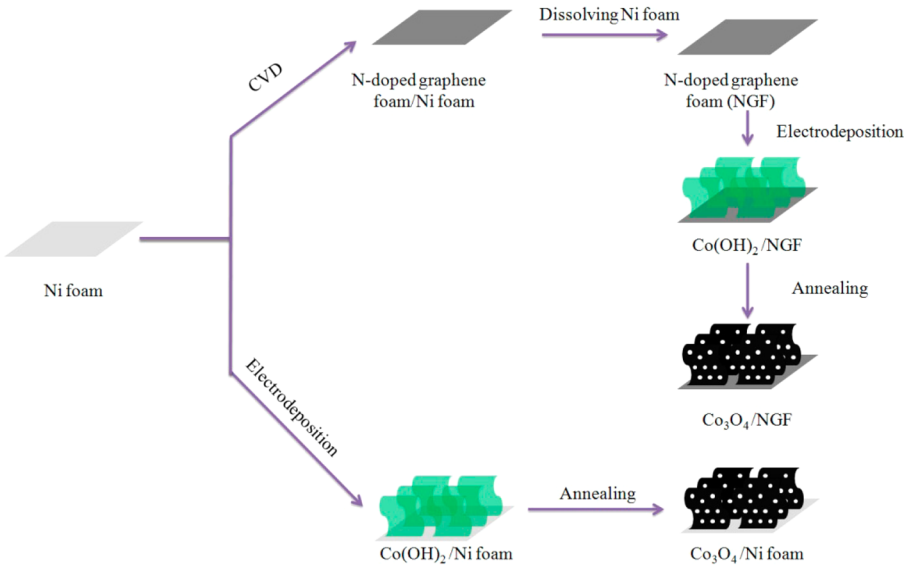


**Figure 1.** Schematic depiction of the synthesis of $Co_3O_4$/NGF and $Co_3O_4$/Ni foam.

Furthermore, it is essential to develop a desirable electrode architecture, which not only favors the penetration of electrolytes into the whole electrode matrix, but also reduces electrical resistance in both the electroactive materials and at the interface between the active material and the current collector.

Graphene, a two-dimensional (2D) monolayer of $sp^2$-hybridized carbon atoms, has attracted enormous interest in recent years because of its extraordinary electrical properties, unusual mechanical strength, and high specific surface area.[12] Various production methods of graphene including mechanical cleavage,[12] epitaxial growth,[13] liquid-phase exfoliation,[14] and chemical vapor deposition (CVD)[15] have been developed recently, which have promoted the intensive study of graphene-based materials in numerous applications, such as field-effect transistors,[16] biological/chemical sensors,[17] and energy storage/conversion devices.[18] In addition, three-dimensional (3D) graphene materials have been widely investigated as active material for SCs,[19,20] since they not only have excellent electrical conductivity, but also provide enhanced surface area. Furthermore, it has been reported that nitrogen doping (or other heteroatom doping) increases the capacitance of graphene due to the modified electronic properties and the induced pseudocapacitance, in addition to the electrical double-layer capacitance.[21]

On the basis of the above considerations, one potential electrode morphology would be a self-supported and binder-free nanoarray structure, which is commonly constructed by one-dimensional (1D) and/or 2D building blocks and directly grown upon 3D current collectors. Various advantages are anticipated for this type of electrode: good electrical conductivity, low diffusion resistance to ionic species, easy electrolyte penetration, and high electroactive surface area. Thus, a short pathway for both ions and electrons is simultaneously constructed to facilitate efficient energy storage at high rates, realizing maximum utilization of electroactive materials at large current loading for this type of electrode.

In this work, a novel bottom-up design of 3D high-performance electrodes, namely mesoporous vertical $Co_3O_4$ nanosheet arrays supported on CVD grown nitrogen-doped graphene foam, is demonstrated. The 3D NGFs are continuous and function as a highly conductive graphene network. Serving as a free-standing monolithic electrode, this material demonstrates improved performance compared to the previously reported $Co_3O_4$ and graphene composites, suggested for supercapacitor applications.[22−25] To the best of our knowledge, it is the first report of a cobalt oxide and nitrogen doped CVD graphene foam composite with this unique 3D hierarchical structure.

## EXPERIMENTAL SECTION

**Synthesis of NGF.** Nitrogen-doped graphene foam (NGF) was prepared via a CVD process using pyridine as both the carbon and nitrogen source. The nickel foam (MTI Corporation, surface density: 350 g $m^{-2}$) was cleaned by successive sonication for 20 min in ethanol and water. A 1 cm × 3 cm piece of cleaned nickel foam was placed at the center of a fused quartz tube furnace (Lindberg Blue M, inner diameter 22 mm). The furnace tube was evacuated and then heated to 1000 °C with a 40 sccm $H_2$ gas flow under atmospheric pressure. After annealing for 20 min under these conditions, pyridine vapor was introduced into the reactor by passing 40 sccm argon gas flow through a bubbler containing liquid pyridine. The temperature and gas flows were maintained in the furnace tube for 2 h. After the growth period, the Ar gas flow was stopped and the sample was cooled to room temperature under 40 sccm $H_2$ gas flow. Finally, the samples were immersed in 1 M $FeCl_3$ overnight to dissolve the Ni foam and leave the free-standing N-doped graphene foam.

**Preparation of Mesoporous Vertical $Co_3O_4$ Nanosheet/Nitrogen-Doped Graphene Foam ($Co_3O_4$/NGF) Composite.** The electrodeposition was performed in a three-electrode cell consisting of NGF as working electrode, a platinum mesh (Aldrich, 52 mesh, surface area: 2 cm × 2 cm) counter electrode and saturated calomel electrode (SCE) reference electrode at room temperature. The $Co(OH)_2$ was electrodeposited on the graphene foam from a 0.05 M $Co(NO_3)_2{\cdot}H_2O$ aqueous electrolyte using an Autolab potentiostat/galvanostat. The electrodeposition potential was −1.0 V (vs SCE). After 20 min of electrodeposition, the resultant green foam was carefully rinsed several times with deionized water and absolute ethanol and finally dried in air. Then the sample was put in a quartz tube and calcined at 250 °C for 2 h with a heating rate of 1 °C $min^{-1}$ to induce the thermal transformation to mesoporous $Co_3O_4$ nanosheets. The average mass loading of $Co_3O_4$ on NGF and Ni foam is 3.0 mg. The values were carefully weighed after calcination of the electrode materials. The samples, using Ni foam or NGF as the


DOI: 10.1021/acsami.5b05095
ACS Appl. Mater. Interfaces 2015, 7, 22831−22838

working electrodes during the electrodeposition process, are named $Co_3O_4$/Ni foam and $Co_3O_4$/NGF, respectively.

**Characterization.** The resultant products were characterized by powder X-ray diffraction (XRD, Rigaku D/max-2550 V, Cu K$\alpha$ radiation), scanning electron microscopy (SEM, Philips XL30 ESEM-FEG), transmission electron microscopy (TEM, JEOL 2000FX) and high-resolution transmission electron microscopy (HRTEM, JEOL 2000FX). Raman spectroscopy was recorded on a Renishaw Raman spectrometer (RE 04) with an excitation wavelength of 532 nm. X-ray photoelectron spectroscopy (XPS) measurements were performed on an ESCALAB 250Xi spectrometer (ThermoFisher-VG Scientific) using a monochromatized Al Ka X-ray source (1486.6 eV).

**Electrochemical Measurements.** Cyclic voltammetry (CV), galvanostatic charge/discharge (GCD), and electrochemical impedance spectroscopy (EIS) tests were carried out using an Autolab potentiostat/galvanostat using a three-electrode cell. As-prepared composite foam was used as the working electrode directly. Pt mesh (Aldrich, 52 mesh, area: 2 cm × 2 cm) was used as the counter electrode and SCE was used as the reference electrode. The electrolyte was 1 M KOH. The cells were charged and discharged at a constant current in the fixed potential range of 0.0−0.45 V. The applied potential window of CV measurements was in the range of 0.0−0.5 V. The capacitance retention tests were carried out at a constant current density of 1 A $g^{-1}$ from 0.0 to 0.45 V for 1000 cycles. Electrochemical impedance spectroscopy (EIS) measurements were carried out by applying an AC voltage with 5 mV amplitude over a frequency range from 0.01 Hz to 100 kHz at 0 V (vs SCE). The equivalent circuit model is shown in the Figure S1a. $R_s$, $C_{dl}$, $R_{ct}$, $C_p$, and $W$ represent the solution resistance, double-layer capacitance, charge transfer resistance, pseudocapacitance, and Warburg impedance (which shows the influence of diffusion control on the charge transfer process), respectively.

The specific capacitance $C_{spec}$ (F $g^{-1}$) was calculated from the GCD data using the following equations

$$C_{spec} = \frac{I_{discharge}\Delta t}{m\Delta V} \quad (1)$$

where $I_{discharge}$ is the discharge current, $\Delta t$ is the discharge time, $\Delta V$ is the change of potential and $m$ is the mass of cobalt oxide and graphene foam/Ni foam composite.

## RESULTS AND DISCUSSION

The schematic of the synthetic procedure is shown in Figure 1. The cleaned Ni foam was used as the template to grow NGF by the CVD technique, and then the Ni foam was dissolved by 1 M $FeCl_3$ solution to obtain self-supported 3D NGF. The $Co_3O_4$/NGF composite was prepared by the electrodeposition and annealing process. As noted above, the $Co_3O_4$/Ni foam composite was prepared using Ni foam as the working electrode, instead of NGF, during the electrodeposition process.

The morphology and structure of the NGF and $Co_3O_4$/NGF were probed by scanning electron microscopy (SEM), as shown in Figure 2. The graphene foam is a 3D hollow structure with a smooth and thin graphene skeleton, as shown in Figure 2a. The width of the graphene skeleton is about 100 $\mu$m. The structure is hollow as confirmed by the high magnification SEM. After the electrodeposition and annealing process, the graphene skeleton was covered by a layer of $Co_3O_4$ nanosheet arrays (Figure 2b−d). The inner layer is graphene foam and the outer layer is $Co_3O_4$, as indicated by the SEM image and corresponding energy dispersive spectrometer (EDS) mapping of C, Co and O (Figure 2c and Figure S2). The thickness of $Co_3O_4$ layer is about 2.6 $\mu$m, the SEM images of samples with various deposition times are shown in Figure S1. The thickness of the $Co_3O_4$ nanosheet is about 100 nm as shown in the inset of Figure 2c. As can be seen from the higher-magnification SEM image (Figure 2d), the $Co_3O_4$ nanosheets grew vertically on the NGF substrate, forming ordered nanosheet arrays with a highly open and porous structure. The resultant structure should increase the accessibility of the electrolyte ions when used as an electrode for electrochemical capacitors.[5]

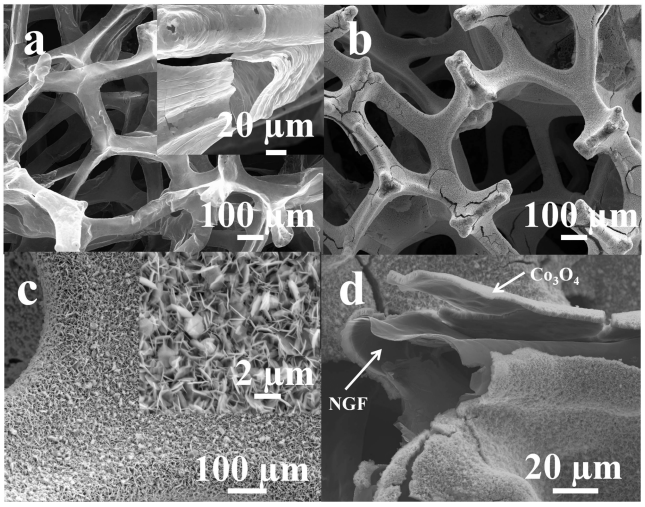


**Figure 2.** (a) SEM images of NGF; (b−d) SEM images of $Co_3O_4$/NGF.

Figure 3a shows the X-ray powder diffraction (XRD) pattern of $Co_3O_4$/NGF composite. The N-doped graphene foam showed two significant diffraction peaks at $2\theta$ = 26.5° and 54.6° attributed to the (002) and (004) reflections of graphitic carbon, respectively.[23] Besides the characteristic peaks from graphene, the $Co_3O_4$/NGF composite presented other diffraction peaks, which were consistent with the (111), (220), (311), (400), (511) and (440) planes in the standard $Co_3O_4$ pattern (JCPDS 42−1467).[23] The Raman spectra of NGF and $Co_3O_4$/NGF composite are shown in Figure 3b. The obvious D peak may be attributed to the N-doping of the sample.[26] Moreover, the characteristic G and 2D peaks were shown in spectra of NGF and $Co_3O_4$/NGF, and the intensity ratio of the G to 2D peaks indicates that the as-grown graphene foams consist of mainly one- to few-layer domains.[27] Finally, four characteristic peaks at 464, 507, 606, and 675 $cm^{-1}$ were identified in the spectrum of the composite, which correspond to $E_g$, $F_{2g}^1$, $F_{2g}^2$, and $A_g^1$ modes of the crystalline $Co_3O_4$.[23] The more detailed elemental composition of $Co_3O_4$/NGF is further characterized by X-ray photoelectron spectrometry (XPS), presented in Figure 3c. All the peaks were corrected to C 1s (284.8 eV). For the XPS survey spectrum, the peaks at around 284.8 eV, 399.8 eV, 530.1 and 795.43 eV can be assigned to the binding energies of C 1s, N 1s, O 1s, and Co 2p.[28] The high-resolution Co 2p XPS spectra of $Co_3O_4$/NGF, as shown in Figure 3d, had two main peaks with binding energies of 781.9 eV (Co $2p_{3/2}$) and 797.3 eV (Co $2p_{1/2}$).[29] The shakeup satellite peak was located at about 6 eV above the main peaks. Above all, the XRD, Raman and XPS characterizations confirm the successful integration of 3D NGF and mesoporous vertical $Co_3O_4$ nanosheet.

$Co_3O_4$ nanosheets, which consists of numerous interconnected nanoparticles forming a mesoporous structure, are generated by the thermal transformation of $Co(OH)_2$ during the annealing process, which was shown by the transmission electron microscopy images (Figure 4a−c). The TEM images


DOI: 10.1021/acsami.5b05095
ACS Appl. Mater. Interfaces 2015, 7, 22831−22838

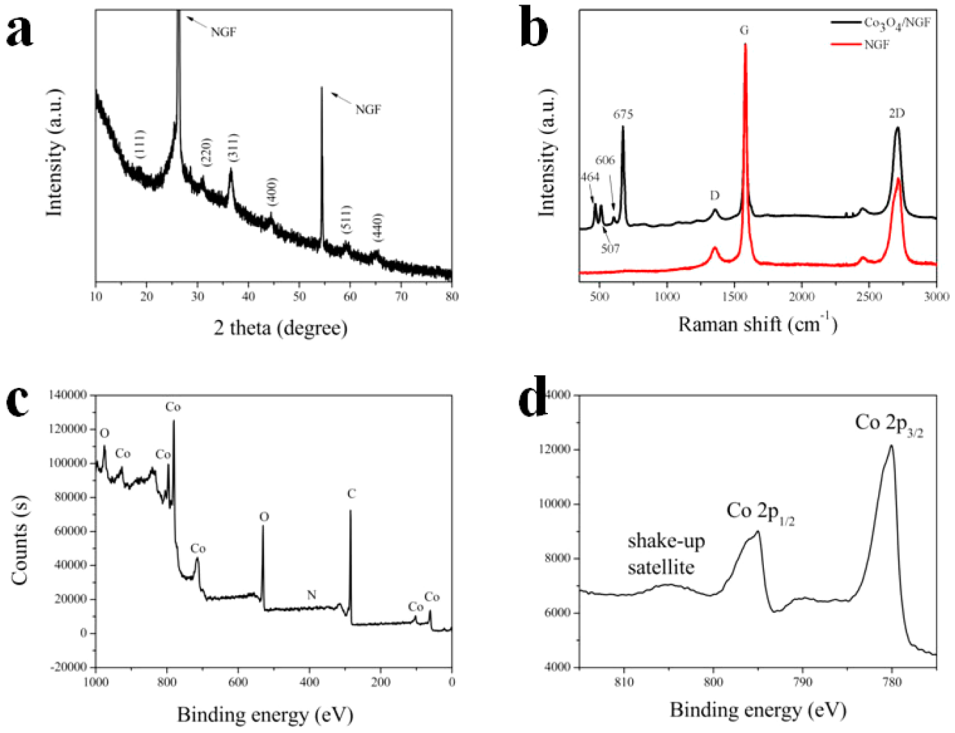


**Figure 3.** (a) XRD pattern of $Co_3O_4$/NGF; (b) Raman spectra of NGF and $Co_3O_4$/NGF; (c) XPS spectrum of $Co_3O_4$/NGF; (d) high-resolution Co 2p XPS spectrum of $Co_3O_4$/NGF.

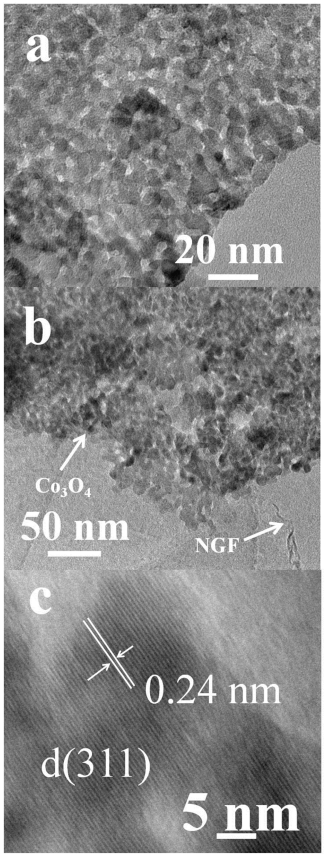


**Figure 4.** (a) TEM image of $Co_3O_4$; (b) TEM image of $Co_3O_4$/NGF; (c) HRTEM image of $Co_3O_4$.

of $Co_3O_4$/Ni foam (Figure 4a) and $Co_3O_4$/NGF (Figure 4b) prove numerous crystalline $Co_3O_4$ nanoparticles, with diameters in the 8−10 nm range, exist along with interparticle mesopores with diameters between 3 and 8 nm. The surface area of the sample is 42 $m^2$ $g^{-1}$ and the pore size, from BET analysis of the nitrogen adsorption and desorption isotherm, is 3−8 nm, which is in broad agreement with the TEM results. The lattice fringes show an interplanar spacing of 0.24 nm in Figure 4c, which agrees with the (311) plane of the cubic $Co_3O_4$.[5]

To investigate the electrochemical performance of the samples, cyclic voltammetry (CV), galvanostatic charge/discharge measurement (GCD) and electrochemical impedance spectroscopy (EIS) were carried out in 1 M KOH with a three-electrode cell. Figure 5a presents the CV data recorded over the potential window from 0 to 0.5 V for $Co_3O_4$/NGF, $Co_3O_4$/Ni foam, and NGF at a scan rate of 20 mV $s^{-1}$. This potential range was chosen as at potentials more positive than 0.5 V, the electrode material was found to break. Moreover, when the potential was extended to potentials below 0 V, the composite capacitance was mainly derived from the double layer capacitance of the material, which lowers the capacitance over the whole potential range, and thus in this work, the potential range 0 to 0.5 V was chosen. No redox peaks were observed during the anodic and cathodic sweeps of NGF. The form of the voltammetric response for $Co_3O_4$/NGF agrees with previous studies on $Co_3O_4$ in KOH solution.[30−32] The redox peaks correspond to the conversion between different cobalt oxidation states, in the case of oxidation, the two sequential reactions are described as follows

$$Co_3O_4 + OH^- + H_2O \leftrightarrow 3CoOOH + e^- \quad (2)$$

$$CoOOH + OH^- \leftrightarrow CoO_2 + H_2O + e^- \quad (3)$$



DOI: 10.1021/acsami.5b05095
ACS Appl. Mater. Interfaces 2015, 7, 22831−22838

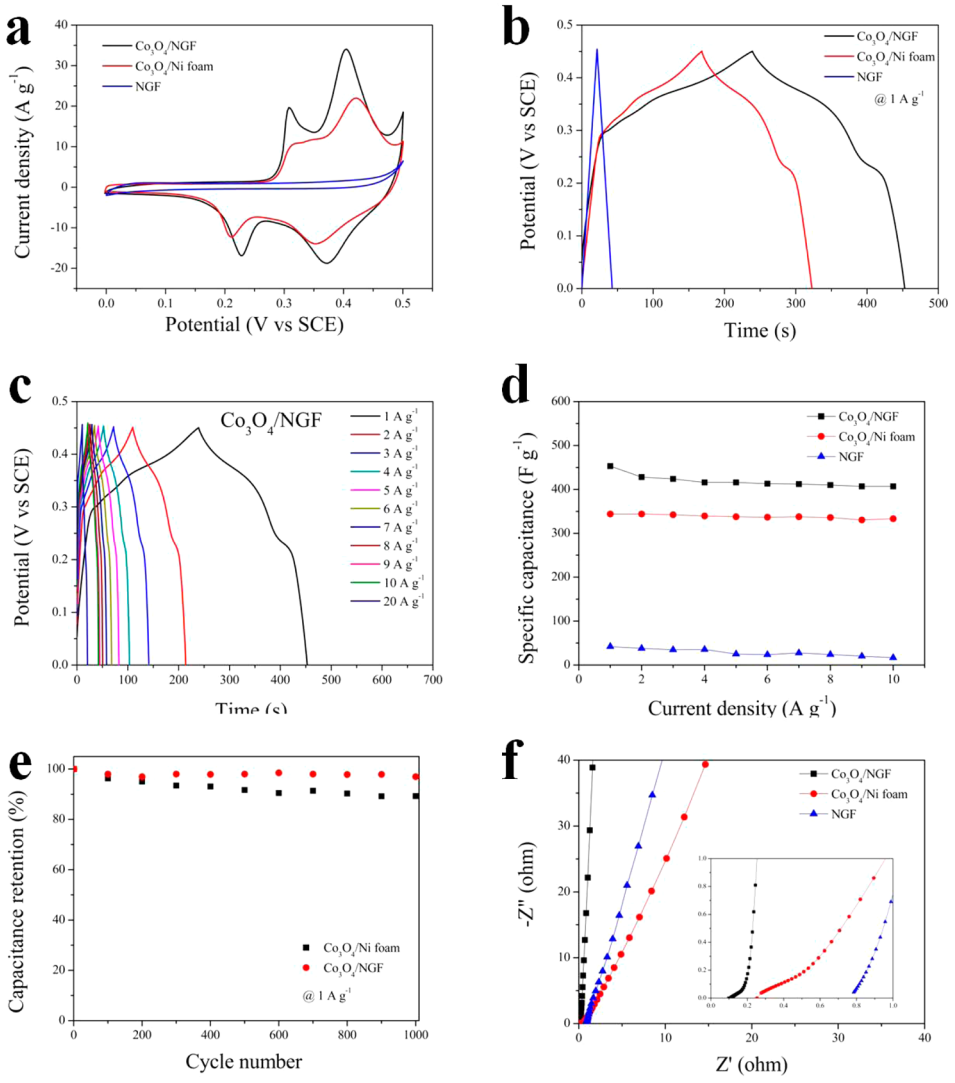


**Figure 5.** Electrochemical performance of NGF, $Co_3O_4$/Ni foam, and $Co_3O_4$/NGF composite using three electrode cell in 1 M KOH. (a) CVs of as-prepared samples at the scan rate of 20 mV $s^{-1}$. (b) Galvanostatic charge/discharge curves of as-prepared samples at discharge current density of 1 A $g^{-1}$. (c) Galvanostatic charge/discharge curves of $Co_3O_4$/NGF at different current densities. (d) Specific capacitance of as-prepared samples at different discharge current densities. (e) Cycle performance of as-prepared samples at discharge current density of 1 A $g^{-1}$. (f) Nyquist plots of as-prepared samples (0.01 Hz to 100 kHz, with an AC amplitude of 5 mV).

Moreover, the area under the CV of $Co_3O_4$/NGF is larger than that of $Co_3O_4$/Ni foam and NGF, which indicates a large synergistic capacitance associated with the $Co_3O_4$/NGF composite electrode. The CVs of $Co_3O_4$/NGF, $Co_3O_4$/Ni foam and NGF at various scan rates are shown in Figure S2b–d.

The improved charge storage properties of the materials can also be observed in galvanostatic charge/discharge (GCD) curves which are shown in Figure 5b. Specifically, treating the charge stored as a capacitance gave an improvement from 320 F $g^{-1}$ (for $Co_3O_4$/Ni foam electrode) to 451 F $g^{-1}$ after introducing NGF at a current density of 1 A $g^{-1}$. Given the promising electrochemical properties of the $Co_3O_4$/NGF composite seen at a current density of 1 A $g^{-1}$, their properties were measured at different current densities. Figures 5c and Figure S1e, f show the GCD curves of $Co_3O_4$/NGF, $Co_3O_4$/Ni foam composite, and NGF at galvanostatic current densities of 1–10 A $g^{-1}$ in the potential range of 0.0 to 0.45 V. The shape of the discharge curves shows the characteristic pseudocapacitance, in agreement with the results from CV. It is worth noting that the capacitance of $Co_3O_4$/NGF composite is 260 F $g^{-1}$ at current density of 20 A $g^{-1}$, which shows a promising high rate performance.

Figure 5d shows the dependence of the specific capacitance of as-prepared samples at current densities from 1 to 10 A $g^{-1}$. Due to the synergistic effects of Faradaic reaction and N-doping, the capacitance retention of the $Co_3O_4$/NGF composite is 88% when the current density was increased from 1 to 10 A $g^{-1}$, indicating that the $Co_3O_4$/NGF composite electrode shows a good rate capability. The electrochemical stability of the as-prepared samples were also evaluated using the galvanostatic charge–discharge technique at a current density of 1 A $g^{-1}$ (Figure 5e).The capacitance retention of $Co_3O_4$/NGF composite is 95% after 1000 cycles while that of $Co_3O_4$/Ni Foam composite is only 89%. Other metal oxide/hydroxide and Ni foam/graphene foam composites have been reported as electrode materials for supercapacitors.[32−36] For example, Ji et al. reported a $Ni(OH)_2$/graphene foam composite as the electrode for supercapacitor. The retention of capacitance is 67% from 0.5 to 10 A $g^{-1}$ in 6 M KOH


DOI: 10.1021/acsami.5b05095
ACS Appl. Mater. Interfaces 2015, 7, 22831−22838

electrolyte solution and capacitance decreased to 65% after 1000 cycles at a current density of 10 A $g^{-1}$.[35] In addition, Yuan et al. prepared a $Co_3O_4$ and Ni foam composite and claimed a high resultant specific capacitance at low current density (based on the mass of $Co_3O_4$); however, the retention of capacitance was only 54% when the current density increased from 2 to 10 A $g^{-1}$.[5] Taken together, our results demonstrate that $Co_3O_4$/NGF composite gives a good rate capability and considerable cycling stability.

Electrochemical impedance spectroscopy (EIS) was employed to characterize the as-prepared samples. Nyquist plots in Figure 5f displays a semicircle in the high-frequency region and a straight line at the low frequency region. The equivalent circuit model fitted with the NOVA software of the potentiostat is shown in Figure S3f and the parameters fitted from the EIS spectra are listed in Table S1.[37,38] The equivalent series resistance (ESR) of the $Co_3O_4$/NGF composite is 0.15 Ω (inset of Figure 5f), which is lower than that of the $Co_3O_4$/Ni foam composite (0.31 Ω), indicating a lower solution resistance and Faradaic resistance. The linear portion corresponds to Warburg impedance, related to the diffusion of electrolyte to the pores of the electrode. The $Co_3O_4$/NGF composite electrode shows the capacitive nature (vertical line for an ideal capacitor) at the low frequency region.

The capacitance of the $Co_3O_4$/NGF composite is much larger than the individual capacitances of $Co_3O_4$ (320 F $g^{-1}$) and that of NGF (42 F $g^{-1}$), which is consistent with other literature.[23] Compared with reduced graphene oxide, the reported capacitance of CVD graphene is low in many literature reports, which can be attributed to the lower defect content and higher proportion of basal plane atoms. Thus, the electrochemical activity is less than that of reduced graphene oxide. For example, the capacitance of CVD graphene and $MnO_2$ composite has been quoted as 29.8 F $g^{-1}$.[39] Lee et al. reported the capacitance of CVD graphene is 59.2 F $g^{-1}$ at a scan rate of 1000 mV $s^{-1}$.[40] Thus, the majority of the measured apparent capacitance originates from the Faradaic component due to the oxide, indicating the efficient utilization of the electroactive of $Co_3O_4$. The outstanding charge storage performance of the mesoporous vertical $Co_3O_4$ arrays on the nitrogen-doped graphene foam electrode can be attributed to its novel structure. First, the mesoporous $Co_3O_4$ nanosheets grown vertically on the NGF not only provide a path for fast electron transport, but also increase the conductivity of the electrode because of the binder-free preparation process of electrode. Meanwhile, the vertical structure can bring many benefits, such as low diffusion resistance to ionic species, easy electrolyte penetration, and large electroactive area.[5] In this way, it can enhance the rate of ion and electron transport in electrodes, and at the electrode−electrolyte interface, and engage sufficient electroactive species exposed on the surface for Faradaic redox reaction. Second, nitrogen-doped graphene foam is a light, high surface area and highly conductive 3D structure. On one hand, the defect-free graphene foam can provide highly conductive pathways to ensure fast charge transfer and conduction.[39] On the other hand, bare graphene foams have been reported to have specific surface area as high as 850 $m^2$ $g^{-1}$, which is much higher than the specific surface area of Ni foam.[41] Third, nitrogen doping can enhance the capacitance of graphene due to the modified electronic properties and the induced pseudocapacitance in addition to the electrical double layer capacitance.[21] Finally, the $Co_3O_4$/NGF composite induces bond formation between $Co_3O_4$ and NGF, with changes in the chemical bonding environment for C, O and Co atoms in the hybrid material claimed to be responsible for the synergistic ORR catalytic activity of $Co_3O_4$ hybrid structures based on N-doped reduced graphene oxide.[28] These factors could also cause the improved charge storage of the $Co_3O_4$/NGF composite.

## CONCLUSION

In summary, a facile route has been employed to fabricate a well-designed $Co_3O_4$/NGF electrode with the aim of achieving enhanced charge storage using this type of material. Treating the charge as pseudocapacitive gives an enhancement in performance from 320 F $g^{-1}$ for $Co_3O_4$/Ni foam to 451 F $g^{-1}$ for $Co_3O_4$/NGF. The synthesis includes growth of NGF on Ni foam by CVD, electrodeposition of $Co(OH)_2$ on the NGF and subsequent thermal transformation to mesoporous $Co_3O_4$ nanosheets. Our physical characterizations demonstrate that the $Co_3O_4$/NGF composite has a unique 3D hierarchical structure and the $Co_3O_4$ nanosheets are mesoporous with pore sizes of 3 to 8 nm. The good charge storage performance of the $Co_3O_4$/NGF electrode was retained, even at current densities of 20 A $g^{-1}$ and the retention factor for the $Co_3O_4$/NGF composite was 95% after 1000 cycles, which also attributed to the 3D hierarchical structure and the synergistic effect between cobalt oxide and nitrogen-doped graphene. The present study shows that high-performance electrode materials can be made with properly designed electrodes based on advanced structures and electroactive materials. Furthermore, the present electrode design can be readily extended to other electroactive materials and their composites.

## ASSOCIATED CONTENT

### Supporting Information

The Supporting Information is available free of charge on the ACS Publications website at DOI: 10.1021/acsami.5b05095.

SEM images of samples with various deposition time; specific capacitance of $Co_3O_4$ samples at different current densities; electrochemical performance of $Co_3O_4$/Ni foam and $Co_3O_4$/NGF composite using a three electrode cell in 1 M KOH; SEM images and corresponding EDS mapping of C, Co, and O and the table of parameters fitted from EIS spectra (PDF)

## AUTHOR INFORMATION

### Corresponding Author

*E-mail: robert.dryfe@manchester.ac.uk. Fax: +44 161 275 4598.

### Author Contributions

The manuscript was written through contributions of all authors. All authors have given approval to the final version of the manuscript.

### Notes

The authors declare no competing financial interest.

## ACKNOWLEDGMENTS

We thank EPSRC (grant ref: EP/K016954/1) for support and the University of Manchester President's Doctoral Scholarship for a studentship for Y.Z.

## ABBREVIATIONS

NGF, nitrogen-doped graphene foam



DOI: 10.1021/acsami.5b05095
ACS Appl. Mater. Interfaces 2015, 7, 22831−22838

SCs, supercapacitors
EDLCs, electrochemical double layer capacitors
PCs, pseudocapacitors
2D, two-dimensional
CVD, chemical vapor deposition
3D, three-dimensional
1D, one-dimensional
$Co_3O_4$/NGF, $Co_3O_4$ nanosheet/nitrogen-doped graphene foam
XRD, X-ray diffraction
SEM, scanning electron microscopy
TEM, transmission electron microscopy
HRTEM, high-resolution transmission electron microscopy
XPS, X-ray photoelectron spectroscopy
CV, Cyclic voltammetry
GCD, galvanostatic charge/discharge
EIS, electrochemical impedance spectroscopy
EDS, energy-dispersive spectrometer

## REFERENCES


(1) Conway, B. E. *Electrochemical Supercapacitors: Scientific Fundamental and Technological Applications*; Kluwer Academic/Plenum: New York, 1999.
(2) Simon, P.; Gogotsi, Y. Materials for Electrochemical Capacitor. *Nat. Mater.* **2008**, *7*, 845−854.
(3) Augustyn, V.; Simon, P.; Dunn, B. Pseudocapacitive Oxide Materials for High-rate Electrochemical Energy Storage. *Energy Environ. Sci.* **2014**, *7*, 1597−1614.
(4) Kumar, N. A.; Choi, H.; Shin, Y. R.; Chang, D. W.; Dai, L.; Baek, J. B. Polyaniline-grafted Reduced Graphene Oxide for Efficient Electrochemical Supercapacitors. *ACS Nano* **2012**, *6*, 1715−1723.
(5) Yuan, C.; Yang, L.; Hou, L.; Shen, L.; Zhang, X.; Lou, X. Growth of Ultrathin Mesoporous $Co_3O_4$ Nanosheet Arrays on Ni Foam for High-performance Electrochemical Capacitors. *Energy Environ. Sci.* **2012**, *5*, 7883−7887.
(6) Brousse, T.; Ɓelanger, D.; Long, J. To Be or Not To Be Pseudocapacitive? *J. Electrochem. Soc.* **2015**, *162*, A5185−A5189.
(7) Simon, P.; Gogotsi, Y.; Dunn, B. Where Do Batteries End and Supercaoacitors Begin. *Science* **2014**, *343*, 1210−1211.
(8) Lan, D.; Chen, Y.; Chen, P.; Chen, X.; Wu, X.; Pu, X.; Zeng, Y.; Zhu, Z. Mesoporous CoO Nanocubes @ Continuous 3D Porous Carbon Skeleton of Rose-Based Electrode for High-Performance Supercapacitor. *ACS Appl. Mater. Interfaces* **2014**, *6*, 11839−11845.
(9) Lei, Y.; Li, J.; Wang, Y.; Gu, L.; Chang, Y.; Yuan, H.; Xiao, D. Rapid Microwave-Assisted Green Synthesis of 3D Hierarchical Flower-Shaped $NiCo_2O_4$ Microsphere for High-Performance Supercapacitor. *ACS Appl. Mater. Interfaces* **2014**, *6*, 1773−1780.
(10) Rakhi, R. B.; Chen, W.; Hedhili, M. N.; Cha, D.; Alshareef, H. N. Enhanced Rate Performance of Mesoporous $Co_3O_4$ Nanosheet Supercapacitor Electrodes by Hydrous $RuO_2$ Nanoparticle Decoration. *ACS Appl. Mater. Interfaces* **2014**, *6*, 4196−4206.
(11) Madhu, R.; Veeramani, V.; Chen, S.; Manikandan, A.; Lo, A.; Chueh, Y. Honeycomb-like Porous Carbon−Cobalt Oxide Nanocomposite for High-Performance Enzymeless Glucose Sensor and Supercapacitor Applications. *ACS Appl. Mater. Interfaces* **2015**, *7*, 15812−15820.
(12) Novoselov, K. S.; Geim, A. K.; Morozov, S. V.; Jiang, D.; Zhang, Y.; Dubonos, S. V.; Grigorieva, I. V.; Firsov, A. A. Electric Field Effect in Atomically Thin Carbon Films. *Science* **2004**, *306*, 666−669.
(13) Sutter, P. W.; Flege, J. I.; Sutter, E. A. Epitaxial Graphene on Ruthenium. *Nat. Mater.* **2008**, *7*, 406−411.
(14) Li, D.; Muller, M. B.; Gilje, S.; Kaner, R. B.; Wallace, G. G. Processable Aqueous Dispersions of Graphene Nanosheets. *Nat. Nanotechnol.* **2008**, *3*, 101−105.
(15) Li, X.; Cai, W.; An, J.; Kim, S.; Nah, J.; Yang, D.; Piner, R.; Velamakanni, A.; Jung, I.; Tutuc, E.; Banerjee, S. K.; Colombo, L.; Ruoff, R. S. Large-Area Synthesis of High-Quality and Uniform Graphene Films on Copper Foils. *Science* **2009**, *324*, 1312−1314.
(16) He, Q.; Wu, S.; Gao, S.; Cao, X.; Yin, Z.; Li, H.; Chen, P.; Zhang, H. Transparent, Flexible, All-Reduced Graphene Oxide Thin Film Transistors. *ACS Nano* **2011**, *5*, 5038−5044.
(17) Srivastava, R. K.; Srivastava, S. T.; Narayanan, N.; Mahlotra, B. D.; Vajtai, R.; Ajayan, P. M.; Srivastava, A. Functionalized Multilayered Graphene Platform for Urea Sensor. *ACS Nano* **2012**, *6*, 168−175.
(18) Zou, Y.; Kinloch, I. A.; Dryfe, R. A. W. Nitrogen-doped and Crumpled Graphene Sheets with Improved Supercapacitance. *J. Mater. Chem. A* **2014**, *2*, 19495−19499.
(19) Cao, X.; Yin, Z.; Zhang, H. Three-dimensional Graphene Materials: Preparation, Structures and Application in Supercapacitors. *Energy Environ. Sci.* **2014**, *7*, 1850−1865.
(20) Yang, J.; Yu, C.; Fan, X.; Qiu, J. 3D Architecture Materials Made of NiCoAl-LDH Nanoplates Coupled with NiCo-carbonate Hydroxide Nanowires Grown on Flexible Graphite Paper for Asymmetric Supercapacitors. *Adv. Energy Mater.* **2014**, *4*, 1400761−1400768.
(21) Wood, K. N.; O'Hayre, R.; Pylypenko, S. Recent Progress on Nitrogen/carbon Structures Designed for Use in Energy and Sustainability Applications. *Energy Environ. Sci.* **2014**, *7*, 1212−1249.
(22) Zhou, W.; Liu, J.; Chen, T.; Tan, K. S.; Jia, X.; Luo, Z.; Cong, C.; Yang, H.; Li, C. M.; Yu, T. Fabrication of $Co_3O_4$-reduced Graphene Oxide Scrolls for High-performance Supercapacitor Electrodes. *Phys. Chem. Chem. Phys.* **2011**, *13*, 14462−14465.
(23) Dong, X.; Xu, H.; Wang, X.; Huang, Y.; Chan-Park, M. B.; Zhang, H.; Wang, L.; Huang, W.; Chen, P. 3D Graphene−Cobalt Oxide Electrode for High-Performance Supercapacitor and Enzymeless Glucose Detection. *ACS Nano* **2012**, *6*, 3206−3213.
(24) Ma, L.; Zhou, H.; Shen, X.; Chen, Q.; Zhu, G.; Ji, Z. Facile Synthesis of $Co_3O_4$ Porous Nanosheets/reduced Graphene Oxide Composites and Their Excellent Supercapacitor Performance. *RSC Adv.* **2014**, *4*, 53180−53187.
(25) Yuan, J.; Zhu, J.; Bi, H.; Meng, X.; Liang, S.; Zhang, L.; Wang, X. Graphene-based 3D Composite Hydrogel by Anchoring $Co_3O_4$ Nanoparticles with Enhanced Electrochemical Properties. *Phys. Chem. Chem. Phys.* **2013**, *15*, 12940−12945.
(26) Ji, H.; Zhao, X.; Qiao, Z.; Jung, J.; Zhu, Y.; Lu, Y.; Zhang, L.; MacDonald, A. H.; Ruoff, R. S. Capacitance of Carbon-based Electrical Double-layer Capacitors. *Nat. Commun.* **2014**, *5*, 3317−3324.
(27) Malard, L. M.; Pimenta, M. A.; Dresselhaus, G.; Dresselhaus, M. S. Raman Spectroscopy in Graphene. *Phys. Rep.* **2009**, *473*, 51−87.
(28) Liang, Y.; Li, Y.; Wang, H.; Zhou, J.; Wang, J.; Regier, T.; Dai, H. $Co_3O_4$ Nanocrystals on Graphene as a Synergistic Catalyst for Oxygen Reduction Reaction. *Nat. Mater.* **2011**, *10*, 780−786.
(29) Biesinger, M. C.; Payne, B. P.; Grosvenor, A. P.; Lau, L. W. M.; Gerson, A. R.; Smart, R.; St, C. Resolving Surface Chemical States in XPS Analysis of First Row Transition Metals, Oxides and Hydroxides: Cr, Mn, Fe, Co and Ni. *Appl. Surf. Sci.* **2011**, *257*, 2717−2730.
(30) Wang, Y.; Lei, Y.; Li, J.; Gu, L.; Yuan, H.; Xiao, D. Synthesis of 3D-Nanonet Hollow Structured $Co_3O_4$ for High Capacity Supercapacitor. *ACS Appl. Mater. Interfaces* **2014**, *6*, 6739−6747.
(31) Zhang, F.; Yuan, C.; Lu, X.; Zhang, L.; Che, Q.; Zhang, X. Facile Growth of Mesoporous $Co_3O_4$ Nanowire Arrays on Ni Foam for High Performance Electrochemical Capacitors. *J. Power Sources* **2012**, *203*, 250−256.
(32) Keng, P.; Kim, B.; Shim, I.; Sahoo, R.; Veneman, P.; Armstrong, N.; Yoo, H.; Pemberton, J.; Bull, M.; Griebel, J.; Ratcliff, E.; Nebesny, K.; Pyun, J. Colloidal Polymerization of Polymer-coated Ferromagnetic Nanoparticles into Cobalt Oxide Nanowires. *ACS Nano* **2009**, *3*, 3143−3157.
(33) Boggio, R.; Carugati, A.; Trasatti, S. Electrochemical Surface Properties of $Co_3O_4$ Electrodes. *J. Appl. Electrochem.* **1987**, *17*, 828−840.
(34) Zhu, Y.; Cao, C.; Tao, S.; Chu, W.; Wu, Z.; Li, Y. Ultrathin Nickel Hydroxide and Oxide Nanosheets: Synthesis, Characterizations and Excellent Supercapacitor Performances. *Sci. Rep.* **2014**, *4*, 5787−5794.



DOI: 10.1021/acsami.5b05095
*ACS Appl. Mater. Interfaces* 2015, 7, 22831−22838

(35) Ji, J.; Zhang, L.; Ji, H.; Li, Y.; Zhao, X.; Bai, X.; Fan, X.; Zhang, F.; Ruoff, R. Nanoporous $Ni(OH)_2$ Thin Film on 3D Ultrathin-Graphite Foam for Asymmetric Supercapacitor. *ACS Nano* **2013**, *7*, 6237−6243.
(36) Gu, L.; Wang, Y.; Lu, R.; Guan, L.; Peng, X.; Sha, J. Anodic Electrodeposition of A Porous Nickel Oxide−hydroxide Film on Passivated Nickel Foam for Supercapacitors. *J. Mater. Chem. A* **2014**, *2*, 7161−7164.
(37) Wang, H.; Qing, C.; Guo, J.; Aref, A. A.; Sun, D.; Wang, B.; Tang, Y. Highly Conductive Carbon−CoO Hybrid Nanostructure Arrays with Enhanced Electrochemical Performance for Asymmetric Supercapacitors. *J. Mater. Chem. A* **2014**, *2*, 11776−11783.
(38) Ghosh, D.; Giri, S.; Das, C. K. Preparation of CTAB-Assisted Hexagonal Platelet $Co(OH)_2$/Graphene Hybrid Composite as Efficient Supercapacitor Electrode Material. *ACS Sustainable Chem. Eng.* **2013**, *1*, 1135−1142.
(39) He, Y.; Chen, W.; Li, X.; Zhang, Z.; Fu, J.; Zhao, C.; Xie, E. Freestanding Three-Dimensional Graphene/$MnO_2$ Composite Networks As Ultralight and Flexible Supercapacitor Electrodes. *ACS Nano* **2013**, *7*, 174−182.
(40) Lee, S.; Lee, S.; Kim, T.; Cho, M.; Yoo, J.; Kim, T.; Lee, Y. Geometry-Controllable Graphene Layers and Their Application for Supercapacitors. *ACS Appl. Mater. Interfaces* **2015**, *7*, 8070−8075.
(41) Chen, Z.; Ren, W.; Gao, L.; Liu, B.; Pei, S.; Cheng, H. Three-dimensional Flexible and Conductive Interconnected Graphene Networks Grown by Chemical Vapour Deposition. *Nat. Mater.* **2011**, *10*, 424−428.


DOI: 10.1021/acsami.5b05095
*ACS Appl. Mater. Interfaces* 2015, 7, 22831−22838